Available online at www.sciencedirect.com
ScienceDirect
Journal of Solid State Chemistry 180 (2007) 533–540
JOURNAL OF SOLID STATE CHEMISTRY
www.elsevier.com/locate/jssc

Chemical bonding in EuTGe (T = Ni, Pd, Pt) and physical properties of EuPdGe

Xavier Rocquefelte[a], Régis Gautier[a], Jean-François Halet[a], Ralf Müllmann[b], Carsten Rosenhahn[b], Bernd D. Mosel[b], Gunter Kotzyba[c], Rainer Pöttgen[c,*]

[a]*UMR 6226 Sciences Chimiques de Rennes, Université de Rennes 1-ENSC Rennes-CNRS, Avenue du Général Leclerc, F-35042 Rennes Cedex, France*
[b]*Institut für Physikalische Chemie, Universität Münster, Corrensstrasse 30, D-48149 Münster, Germany*
[c]*Institut für Anorganische und Analytische Chemie, Universität Münster, Corrensstrasse 30, D-48149 Münster, Germany*

Received 22 September 2006; received in revised form 17 October 2006; accepted 13 November 2006
Available online 17 November 2006

Abstract

EuPdGe was prepared from the elements by reaction in a sealed tantalum tube in a high-frequency furnace. Magnetic susceptibility measurements show Curie–Weiss behavior above 60 K with an experimental magnetic moment of 8.0(1)μ_B/Eu indicating divalent europium. At low external fields antiferromagnetic ordering is observed at $T_N = 8.5(5)$ K. Magnetization measurements indicate a metamagnetic transition at a critical field of 1.5(2) T and a saturation magnetization of 6.4(1)μ_B/Eu at 5 K and 5.5 T. EuPdGe is a metallic conductor with a room-temperature value of $5000 \pm 500\ \mu\Omega$ cm for the specific resistivity. ^{151}Eu Mössbauer spectroscopic experiments show a single europium site with an isomer shift of $\delta = -9.7(1)$ mm/s at 78 K. At 4.2 K full magnetic hyperfine field splitting with a hyperfine field of $B = 20.7(5)$ T is observed. Density functional calculations show the similarity of the electronic structures of EuPdGe and EuPtGe. T–Ge interactions (T = Pd, Pt) exist in both compounds. An ionic formula splitting $Eu^{2+}T^{0}Ge^{2-}$ seems more appropriate than $Eu^{2+}T^{2+}Ge^{4-}$ accounting for the bonding in both compounds. Geometry optimizations of EuTGe (T = Ni, Pt, Pd) show weak energy differences between the two structural types.

Keywords: Intermetallic europium compounds; Magnetism; ^{151}Eu Mössbauer spectroscopy; Chemical bonding

1. Introduction

The equiatomic intermetallic europium compounds EuTX (T = transition metal, X = main group element) have intensively been investigated in recent years with respect to their crystal structures and physical properties [1–7, and ref. therein]. Although a huge number of crystal structures and physical properties have been reported, only little information on chemical bonding in this interesting class of compounds is available. Only the pnictides EuPdP [8], $EuPd_{1-x}Ag_xP$, and $EuPd_{1-x}Au_xAs$ [9] have been investigated by TB-LMTO-ASA band structure calculations in order to elucidate the valence instabilities in more detail. In a recent review article [7], chemical bonding in EuZnGe, EuPdGa, and EuScGe has been discussed.

Herein we report on electronic structure calculations on the germanides EuPdGe (monoclinic EuNiGe type) [10] and EuPtGe (cubic LaIrSi type) [11,12]. Although both germanides have the same electron count, they crystallize with different structure types and exhibit different magnetic properties. Magnetic susceptibility and ^{151}Eu Mössbauer spectroscopic measurements [12] indicate divalent europium in EuPtGe. This germanide remains paramagnetic down to 4.2 K. The physical properties of the palladium compound are reported herein.

2. Experimental

2.1. Synthesis

Starting materials for the preparation of EuPdGe were ingots of europium (Johnson Matthey), palladium powder (Degussa-Hüls, 200 mesh), and germanium lumps

*Corresponding author. Fax: +49 251 83 36002.
E-mail addresses: halet@univ-rennes1.fr (J.-F. Halet), pottgen@uni-muenster.de (R. Pöttgen).

0022-4596/$ - see front matter © 2006 Elsevier Inc. All rights reserved.
doi:10.1016/j.jssc.2006.11.013

(Wacker), all with stated purities greater than 99.9%. The large europium ingots were cut into smaller pieces in a glove-box. They were not allowed to contact air prior to the reactions. The elemental components were mixed in the ideal atomic ratio and sealed in a tantalum tube under an argon pressure of about 800 mbar [13]. The argon was purified over molecular sieves and titanium sponge (900 K).

The tantalum tube was annealed in a water-cooled sample chamber in a high-frequency furnace (Hüttinger Elektronik, Freiburg, TIG 1.5/300) as described in detail in Ref. [14]. In a first step the tube was heated with the maximum power output of the high-frequency generator. The strongly exothermic reactions are easily visible by a heat flash for about 1 s. The annealing temperature was then lowered to about 900 K for about 1 min and then raised again to the maximum. Subsequently the tube was annealed for 2 h at about 900 K. The reaction resulted in a light gray polycrystalline sample of EuPdGe which could easily be separated from the tantalum tube without any tantalum contamination (checked by EDX analyses). Powders of EuPdGe are stable in air. No decomposition was observed after several months.

2.2. X-ray powder diffraction

The purity of the sample was checked by a Guinier powder pattern with Cu $K\alpha_1$ radiation and α-quartz ($a = 491.30$ pm, $c = 540.46$ pm) as an internal standard. The experimental pattern was compared to a calculated one [15] taking the atomic positions from the structure refinement [10]. Only the reflections of monoclinic EuPdGe were observed.

2.3. Physical property measurements

The magnetic susceptibilities of polycrystalline pieces of EuPdGe were determined with a SQUID magnetometer (Quantum Design, Inc.) between 4.2 and 300 K with magnetic flux densities up to 5.5 T. The specific resistivities were measured on small blocks (about $1 \times 1 \times 2\,mm^3$) with a conventional four-probe technique over the temperature range from 4.2 to 300 K. The blocks were directly cut from the sample prepared in the tantalum tube. Cooling and heating curves were identical within the error limits, and reproducible for different samples.

2.4. ^{151}Eu Mössbauer spectroscopy

The 21.53 keV transition of ^{151}Eu with an activity of 130 MBq (2% of the total activity of a ^{151}Sm:EuF_3 source) was used for the Mössbauer spectroscopic experiments. The measurements were performed with a commercial helium bath cryostat. The temperature of the absorber could be varied from 4.2 to 300 K and was measured with a metallic resistance thermometer with accuracy better than ± 0.5 K. The source was kept at room temperature. The material for the Mössbauer spectroscopic measurements was the same as for the susceptibility and resistivity measurements. The sample was placed within a thin-walled PVC container at a thickness corresponding to about 10 mg Eu/cm^2.

2.5. Electronic structure calculations

Self-consistent spin-polarized *ab initio* band structure calculations were performed on EuTGe (T = Ni, Pd, Pt) with the scalar relativistic tight-binding linear muffin–tin orbital (LMTO) method in the atomic spheres approximation including the combined correction [16]. Exchange and correlation were treated in the local density approximation (LDA) using the von Barth-Hedin local exchange correlation potential [17]. Within the LMTO formalism interatomic spaces are filled with interstitial spheres. The optimal positions and radii of these additional "empty spheres" (ES) were determined by the procedure described in Ref. [18]. Nine and ten non-symmetry-related ES with $0.54\,Å \leqslant r_{ES} \leqslant 0.77\,Å$ and $0.58\,Å \leqslant r_{ES} \leqslant 0.84\,Å$ were introduced for the calculations on EuNiGe and EuPdGe, respectively. The full LMTO basis set consisted of 4*f*, 5*d*, 6*s* and 6*p* functions for Eu spheres, 5*f*, 5*d*, 6*s* and 6*p* functions for Pt spheres, 4*d*, 5*s* and 5*p* functions for Pd spheres, 3*d*, 4*s* and 4*p* functions for Ni spheres, 4*s*, 4*p* and 4*d* functions for Ge spheres, and *s* and *p* functions for ES. The eigenvalue problem was solved using the following minimal basis set obtained from the Löwdin downfolding technique: Eu 5*d*, 6*s*, 6*p*; Pt 5*d*, 6*s*, 6*p*; Pd 4*d*, 5*s*, 5*p*; Ni 3*d*, 4*s*, 4*p*; Ge 4*s*, 4*p* and interstitial 1*s* LMTOs. The k space integration was performed using the tetrahedron method [19]. Charge self-consistency and the average properties were obtained from 164, 30, and 64 irreducible k points for EuPtGe, EuPdGe, and EuNiGe, respectively. A measure of the magnitude of the bonding was obtained by computing the crystal orbital Hamiltonian populations (COHP) which are the Hamiltonian population weighted density of states (DOS) [20]. As recommended [21], a reduced basis set (in which all ES LMTOs have been downfolded) was used for the COHP calculations. Bands, DOS, and COHP curves are shifted so that ε_F lies at 0 eV.

Geometry optimizations were performed using the Vienna Ab initio Simulation Package (VASP) [22] based on density functional theory. The wave functions were expanded in a plane-wave basis set with kinetic energy of 400 eV. The VASP package was used with the projector augmented wave (PAW) method of Blöchl [23]. The electronic exchange and correlation were treated in the LDA and corrections were taken into account by the generalized gradient approximation (GGA) exchange and correlation functional of Perdew–Wang [24].

3. Results and discussion

3.1. Crystal chemistry

The crystal chemistry of EuPdGe and EuPtGe was already discussed in detail in the original papers concerning

the structure determinations [10–12]. Herein we focus on the comparison of the two different structure types. Although EuPdGe and EuPtGe have the same electron count, the palladium germanide crystallizes with the monoclinic EuNiGe type structure [25], while the platinum compound adopts the cubic LaIrSi type [26]. Perspective views of both structures are presented in Fig. 1. The europium atoms are the by far most electropositive components of these compounds and they have largely transferred their two valence electrons to the [PdGe] and [PtGe] networks. The formulae of both germanides may, to a first approximation, be written as $Eu^{2+}[PdGe]^{2-}$ and $Eu^{2+}[PtGe]^{2-}$, emphasizing the covalent Pd–Ge and Pt–Ge bonding. Cutouts of the polyanions are presented in Fig. 2.

The [PdGe] polyanion in EuPdGe has a pronounced two-dimensional character. Each palladium (germanium) atom has three germanium (palladium) neighbors at Pd–Ge distances ranging from 245 to 250 pm, slightly smaller than the sum of Pauling's single bond radii [27,28] of 250 pm. The $[PdGe_3]$ group is nearly planar, whereas the $[Pd_3Ge]$ group is somewhat pyramidal. Within the polyanion we observe eight-membered Pd_4Ge_4 rings and Pd_2Ge_2 squares (Fig. 2). Within the distorted squares, the germanium atoms show a maximum separation. This way the palladium atoms get a closer distance of 289 pm, only slightly larger than in *fcc* palladium [29] (Pd–Pd 275 pm), which may indicate weak Pd–Pd interactions.

The [PtGe] polyanion in EuPtGe has a different geometry (Fig. 2). Each platinum atom has three germanium neighbors at equal Pt–Ge distances of 238 pm, significantly smaller than the sum of Pauling's single bond radii [27] of 252 pm, indicating strongly bonding Pt–Ge interactions. Interestingly, an almost planar Y-shape arrangement is noted for both Pt and Ge atoms. Within the polyanion, the platinum and germanium atoms form distorted ten-membered Pt_5Ge_5 rings. Another difference between the two structures concerns the coordination of the europium atoms. In EuPdGe the europium atoms have coordination number (CN) 18 (6 Eu + 6 Pd + 6 Ge), while CN20 (6 Eu + 7 Pt + 7 Ge) is observed in EuPtGe. The six europium neighbors in EuPtGe have the same Eu–Eu distance of 401 pm. In EuPdGe the Eu–Eu distances range from 363 to 421 pm, however, the average Eu–Eu distance of 400 pm compares well with the platinum compound.

3.2. Chemical bonding analysis

Spin-polarized total and atom-projected LMTO DOS of EuPdGe and EuPtGe are sketched in Figs. 3 and 4, respectively. DOS of both compounds show the strong polarization of the seven unpaired 4*f* electrons of the europium atoms. This confirms the formal charge +2 of the rare-earth atoms. Spin polarization hardly affects the other atoms. Spin-up and spin-down projected DOS of these atoms are nearly identical. DOS curves of both compounds are consistent with their metallic electrical properties.

Because of the electronegativity differences, formal charge distribution between metals and main-group atoms often results in a partial electron transfer from the metal to the main-group atoms. In the case of group-14 atoms, the formal charge of the main-group atom is −4. Such a formal charge for germanium atoms would lead to the electron precise formulation $Eu^{2+}T^{2+}Ge^{4-}$, as requested from the Zintl–Klemm concept. However, according to the Pauling electronegativity scale, germanium is slightly less electronegative than palladium and platinum (1.8 vs. 2.2) [27]. This may render inappropriate the charge distribution mentionned above. Indeed, calculation of the electronic occupation of the *d* levels of the *T* atoms (9.30 for Pd and 9.33 electrons for Pt) shows that the formal oxidation state of the transition metals atoms is rather zero in these compounds. Such a formal oxidation state is in turn in agreement with the 16-electron count (10 (Pd or Pt) + 3 × 2 (Ge), generally required for a transition metal in trigonal planar geometry such as the molecular complex $Pt(PPh_3)_3$ [30]. Therefore, the oxidation formalism $Eu^{2+}T^{0}Ge^{2-}$ seems more appropriate than $Eu^{2+}T^{2+}Ge^{4-}$ in accounting

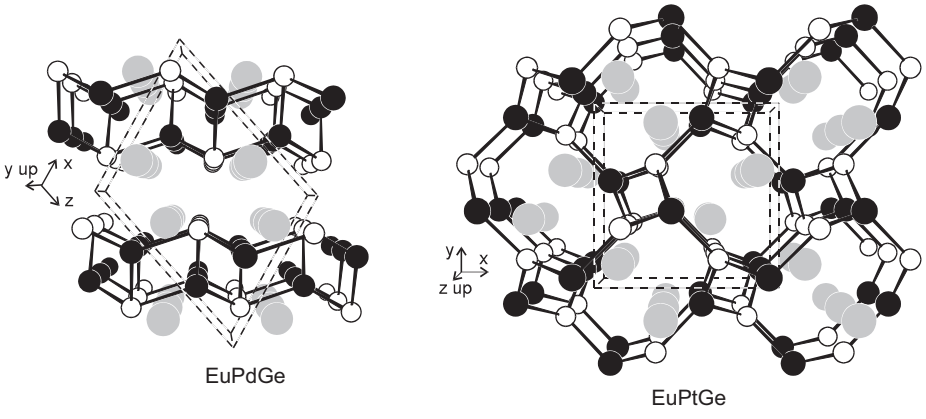

Fig. 1. Perspective views of the monoclinic EuPdGe and cubic EuPtGe structures. The europium, palladium (platinum), and germanium atoms are drawn as large gray, small filled, and medium open circles, respectively. The two-dimensionally, respectively three-dimensional [PdGe] and [PtGe] networks are emphasized.

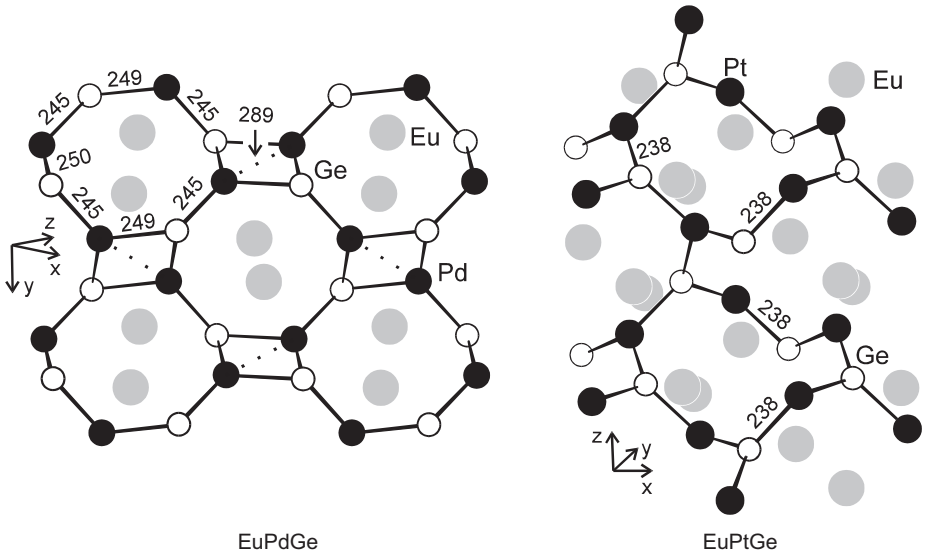

Fig. 2. Cutouts of the [PdGe] and [PtGe] polyanions in the structures of EuPdGe and EuPtGe. Atom designations and some relevant interatomic distances are given.

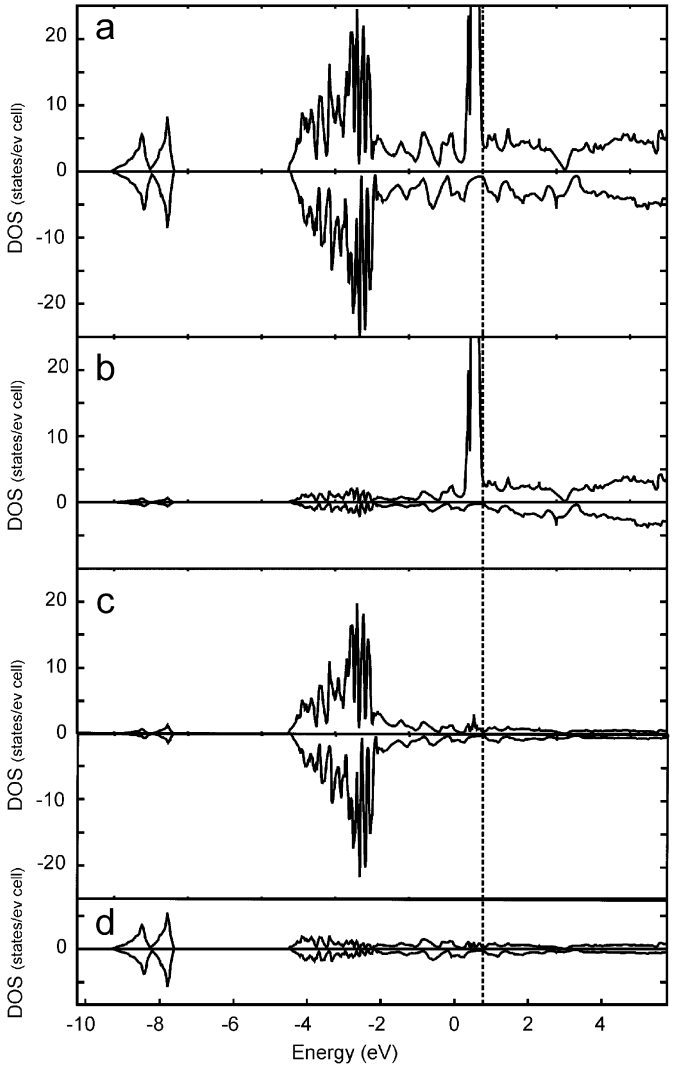

Fig. 3. Spin-polarized DOS of EuPdGe, total (a) and atomic contributions: Eu (b) Pd (c) and Ge (d).

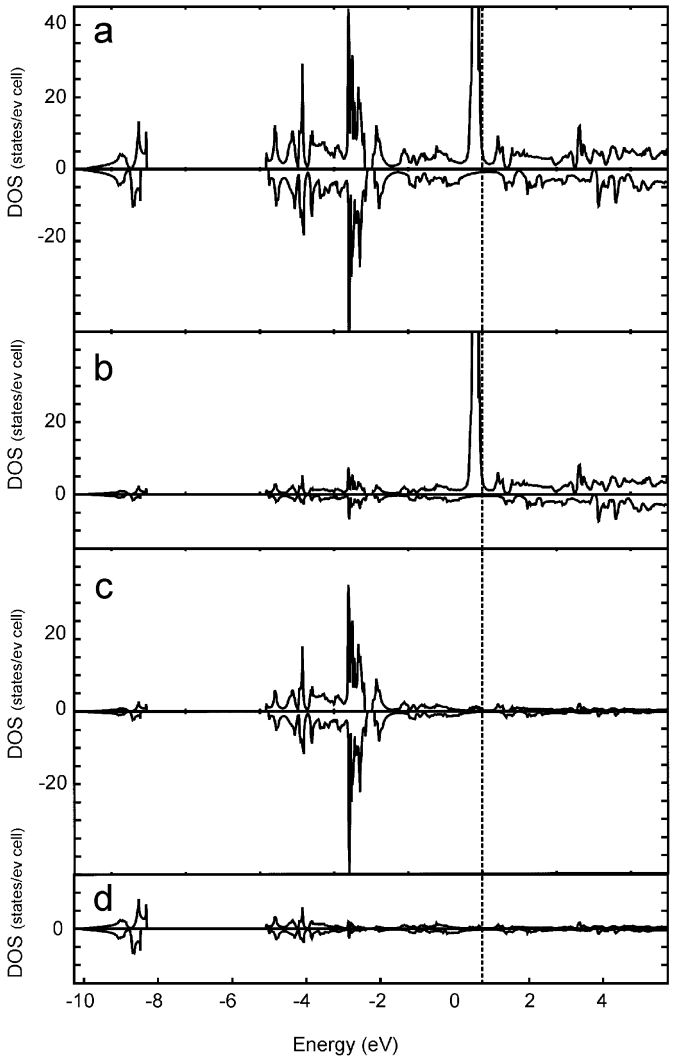

Fig. 4. Spin-polarized DOS of EuPtGe, total (a) and atomic contributions: Eu (b) Pt (c) and Ge (d).

for the *T*–Ge arrangement in both compounds. This leads to formally 6-electron Ge atoms. This is not surprising in EuPtGe since the Ge atoms are trigonally planar. This reminds planar BF_3 with the 6-electron boron atom. This is more puzzling in EuPdGe where the Ge atoms are somewhat pyramidal (even though the Pt–Ge–Pt angles observed are far from equal [10–12]). Additionally, the proposed oxidation formalism (supported by our calculations) is not in agreement at first sight with the relatively short Pd–Pd contacts in EuPdGe. Only *T*–Ge covalent interactions should predominate in these compounds since there are no electrons formally available for other interactions. Pd–Ge and Pd–Pd, and Pt–Ge COHP curves are shown in Figs. 5 and 6, respectively. In both compounds *T*–Ge interactions are maximized with *T*–Ge bonding states occupied and the *T*–Ge antibonding states unoccupied. In EuPdGe, even though a Pd–Pd distance of 289 pm seems consistent with some metal–metal bonding, the Pd–Pd COHP curve indicates a very weak metal–metal interaction with both Pd–Pd bonding and antibonding states being occupied. This reflects indeed the "soft" bonding interaction between the d^{10} metal Pd (0) centers in EuPdGe. Weak d^{10}–d^{10} bonding interactions resulting from a mixing of the *s*, *p*, and *d* levels are quite common in molecular copper chemistry for instance [31].

Further insight in the nature of the bonding in these compounds can be provided by the Electron Localization Function (ELF) [32]. Being directly related to the electron pair probability density, its graphical representation can contribute to the understanding of electron localization. ELF isosurface for EuPdGe corresponding to a value of 0.78 is sketched in Fig. 7. Except for the germanium lone pairs, no localization domains between atoms can be identified. This supports the very weak through-space bonding between palladium atoms in spite of the Pd–Pd distance equal to 289 pm, as well as the metallic behavior of EuPdGe. ELF analysis has also been carried out for EuPtGe. No significant difference can be noted with respect to EuPdGe considering this topologic analysis of the electron density.

For a better understanding of their structural and electronic properties, full geometry optimization of EuPdGe and EuPtGe was carried out for the two structure types using the VASP program. Calculations were also performed for EuNiGe which exhibits the same crystallographic structure than EuPdGe. From GGA calculations (see Table 1), the stability of the Ni and Pd phases is well reproduced, but not for the Pt phase. In other words, regardless of *T*, the EuPdGe structure type is always computed to be more stable when GGA exchange-correlation functional is used. In order to improve the treatment of the Eu atoms and to better describe their f^7 electronic configuration, a Hubbard-U term of 3 eV was added to the GGA treatement [33]. The stability of the three phases is well reproduced. However, it should be noted that the energy differences are quite small. In particular for EuNiGe the two structure types exhibit the same cohesive energy (ca. −18 meV/f.u.).

Optimized volumes are also given in Table 1 and compared to the experimental ones. Interestingly, it appears that the volume per formula unit depends more strongly on the structure type than on the metal for T = Pd and Pt. As an illustration, the GGA optimized volume of EuPdGe and EuPtGe is 65.0 and 65.8 $Å^{-3}$/f.u., respectively with the EuPdGe structure type, while they are 70.2 and 70.3 $Å^{-3}$/f.u., respectively with the EuPtGe structure type.

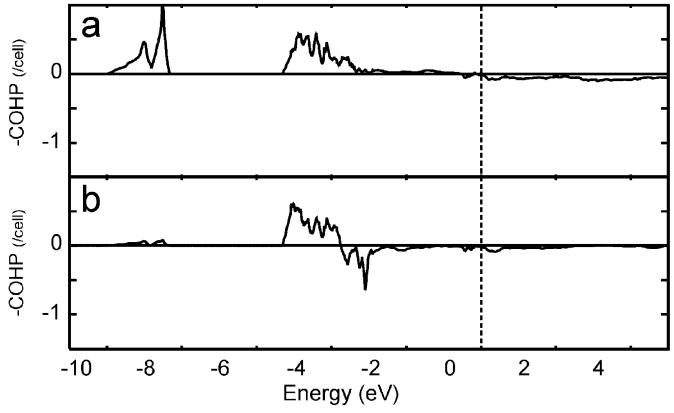

Fig. 5. Pd–Ge (from 2.448 to 2.503 Å) (a) and Pd–Pd (2.892 Å) (b) COHP curves for EuPdGe.

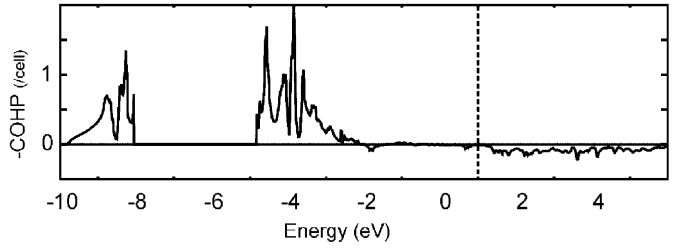

Fig. 6. Pt–Ge (2.380 Å) COHP curve for EuPtGe.

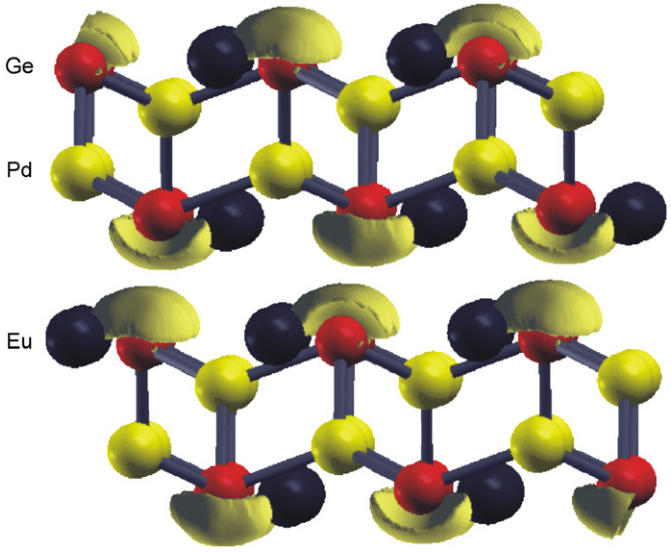

Fig. 7. ELF plot for EuPdGe (contour line $\eta = 0.78$).

Table 1
Energy difference (ΔE) and experimental (V_{EXP}) and optimized (V_{OPT}) volumes for EuTGe compounds

	EuNiGe	EuPdGe	EuPtGe
ΔE (meV/f.u.)	−93/**−18**	−172/**−63**	−67/**48**
V_{EXP} (Å^{-3}/f.u.)	62.6	66.5	70.1
V_{OPT} (Å^{-3}/f.u.)			
EuPdGe structure type	58.6/**63.4**	65.0/**69.1**	65.8/**69.4**
($V_{OPT}-V_{EXP}$)/V_{EXP} (%)	−6.4/+**1.3**	−2.2/+**3.9**	−6.1/−**1.0**
EuPtGe structure type	61.4/**64.2**	70.2/**73.0**	70.3/**72.9**
($V_{OPT}-V_{EXP}$)/V_{EXP} (%)	−1.9/+**2.5**	+5.5/+**9.8**	+0.3/+**4.0**

The energy differences are between the EuPdGe and EuPtGe structure types after optimization of the crystallographic structure. The plain and bold values results from GGA and GGA+U ($U=3$ eV) calculations, respectively.

In contrast, and as expected, significant volume contraction is observed for $T=$ Ni.

3.3. Magnetic and electrical properties of EuPdGe

The temperature dependence of the inverse magnetic susceptibility of EuPdGe measured at external field strength of 2 T is presented in Fig. 8. Above 60 K, EuPdGe shows Curie–Weiss behavior. The experimental magnetic moment determined from this high temperature part of the inverse susceptibility is 8.0(1)μ_B/Eu, in good agreement with the value of 7.94μ_B for the free Eu^{2+} ion. The paramagnetic Curie temperature (Weiss constant) of 12(1) K was obtained by linear extrapolation of the high temperature part (data above 60 K) of the $1/\chi$ vs. T plot to $1/\chi=0$. The inset of Fig. 8 shows the low temperature behavior measured at 0.01 T in the range 4.2–35 K. At low external fields EuPdGe orders antiferromagnetically at $T_N=8.5(5)$ K (minimum of the $1/\chi$ vs. T plot at 0.1 T).

The magnetization vs. external field dependence at 5 K is shown in Fig. 9. The magnetization increases in a linear manner up to about 1.5 T as expected for a paramagnetic material. At the critical field of $B_C=1.5(2)$ T, we observe an increase of the magnetization which is due to a metamagnetic transition (antiferro- to ferromagnetic transition). At the highest obtainable field of 5.5 T, the saturation magnetic moment is $\mu_{sm(exp)}=6.4(1)\mu_B$/Eu, only slightly smaller than the theoretical value of $\mu_{sm(calc)}=7.0\mu_B$/Eu, calculated from $\mu_{sm(calc)}=g\times J\mu_B$ [34]. We have thus achieved an almost parallel spin alignment at 5 K and 5.5 T. Similar high saturation magnetizations have recently also been observed for the metamagnets EuPdIn [35,36], EuPtIn [6], and EuZnSn [37].

The temperature dependence of the specific resistivity of EuPdGe is plotted in Fig. 10. The specific resistivity decreases with decreasing temperature as it is typical for a metal. According to the room temperature value of

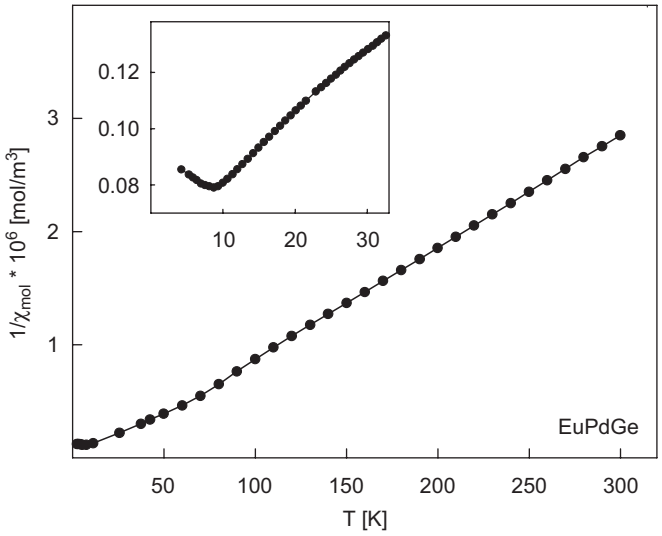

Fig. 8. Temperature dependence of the inverse magnetic susceptibility of EuPdGe measured at a magnetic flux density of 2 T. The inset shows the inverse susceptibility measured at 0.01 T at low temperatures.

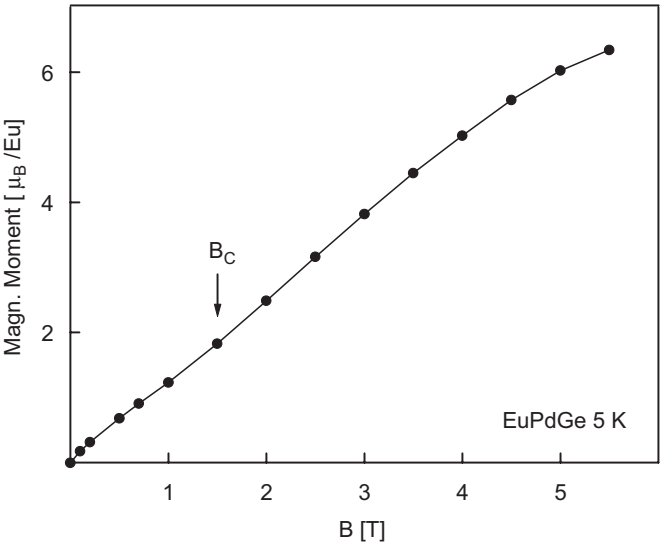

Fig. 9. Magnetization vs. external field dependence of EuPdGe at 5 K.

$5000\pm500\,\mu\Omega$ cm, EuPdGe is a poor conductor. At low temperature, the specific resistivity has dropped to $1500\pm200\,\mu\Omega$ cm. The relatively large standard deviations account for the values obtained for different samples. The large absolute values of the specific resistivity can also result from microcracks within the very brittle samples. The steeper decrease below 10 K is due to the onset of antiferromagnetic ordering, resulting from freezing of spin-disorder scattering.

3.4. ^{151}Eu Mössbauer spectroscopy of EuPdGe

The ^{151}Eu Mössbauer spectra of EuPdGe at 4.2, 8, 10 and 78 K are shown in Fig. 11 together with transmission intergral fits. The fitting parameters are listed in Table 2. No Eu^{III} impurity peak can be detected around $\delta=0$ mm/s

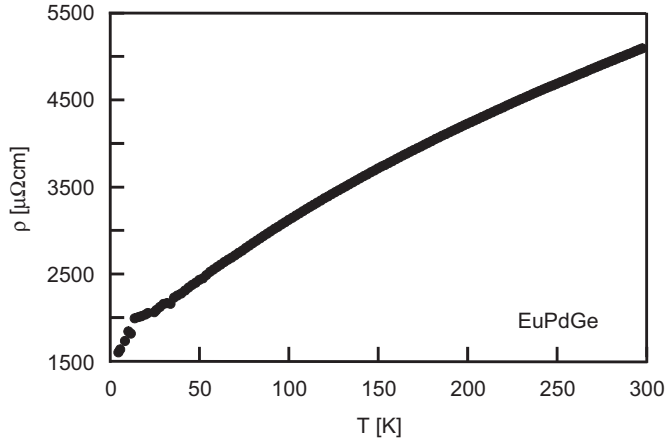

Fig. 10. Temperature dependence of the specific resistivity of EuPdGe.

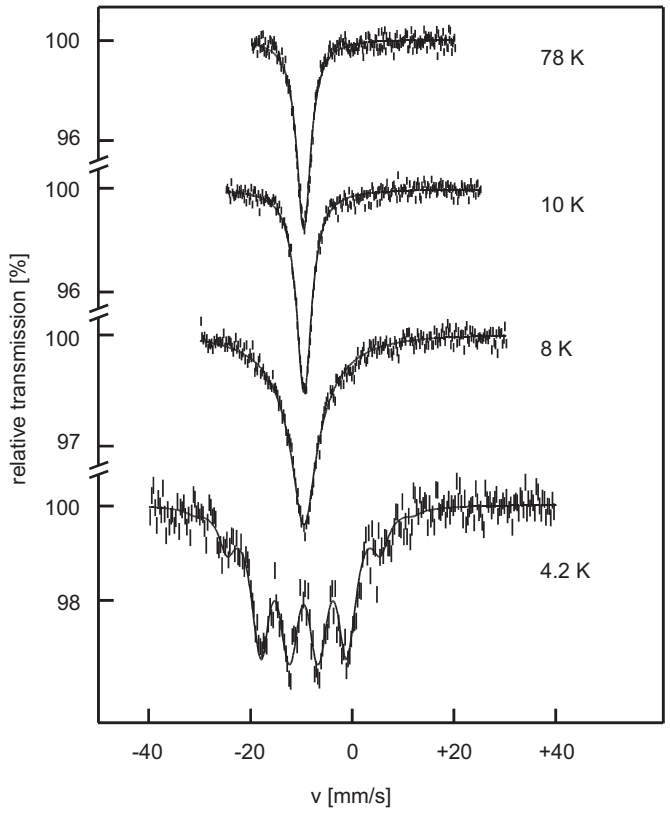

Fig. 11. Experimental and simulated ^{151}Eu Mössbauer spectra of EuPdGe at various temperatures.

indicating pure Eu(II) in the investigated EuPdGe sample. At 78 K the spectrum shows a single signal at $\delta = -9.70(6)$ mm/s with a slightly enlarged line width of $\Gamma = 3.1(2)$ mm/s. The onset of magnetic ordering in EuPdGe is detected at 10 K (increase of the line width) in the ^{151}Eu Mössbauer spectroscopic experiments, slightly higher than the Néel temperature of 8.5(5) K determined from the susceptibility data. At 4.2 K we observe full magnetic hyperfine field splitting with a static magnetic flux density of 20.7(5) T at the europium nuclei.

Table 2
^{151}Eu Mössbauer fitting parameters for EuPdGe as a function of temperature

T (K)	Γ (mm/s)	δ (mm/s)	B (T)
78	3.1(2)	−9.7(1)	—
10	3.2(2)	−9.6(1)	—
8	3.4	−9.7	20.7
4.2	3.4(5)	−9.7(2)	20.7(5)

Note: The numbers in parentheses give the statistical errors in the last digit. Values without parentheses were kept fixed by the fitting program. For the 8 K data a fluctuation frequency of $2.72(8) \times 10^9$ Hz was considered for the fit.
δ, isomer shift with respect to EuF_3; Γ, experimental line width; B, static magnetic flux density.

Two features are worthy to note. The experimental line widths range from 3.1(2) mm/s (78 K) to 3.4(5) mm/s (4.2 K), somewhat larger than the natural line width of 2.3 mm/s of ^{151}Eu. The europium site of EuPdGe has the very low site symmetry 1, suggesting quadrupole splitting. As a test, the 78 K spectrum was also fit with a fixed line width of 2.5 mm/s, resulting in quadrupole splitting of 7.7(8) mm/s. An independent refinement of the line width and the quadrupole parameter was not stable. Both parameters showed large correlations. We therefore preferred to refine the spectra with slightly enlarged line widths. The small quadrupole splitting is then masked behind the larger line width in all spectra.

The second interesting feature concerns the 8 K spectrum, where a fluctuation frequency of $2.72(8) \times 10^9$ Hz was refined. At this temperature near T_N most magnetic moments (about four fifths) show still some fluctuations, while only one fifth of the moments are fully ordered, however, full magnetic hyperfine field splitting is observed at 4.2 K.

Acknowledgments

We thank N. Rollbühler and Dr. R.K. Kremer (MPI FKF, Stuttgart) for the resistivity measurement and the Degussa-Hüls AG for a generous gift of palladium powder. This work was financially supported by the Deutsche Forschungsgemeinschaft. We also thank the Pôle de Calcul Intentif de l'Ouest (PCIO) of the University of Rennes for computing facilities.

References

[1] C. Tomuschat, H.-U. Schuster, Z. Anorg. Allg. Chem. 518 (1984) 161.
[2] J. Evers, G. Oehlinger, K. Polborn, B. Sendlinger, J. Solid State Chem. 91 (1991) 250.
[3] G. Michels, C. Huhnt, W. Scharbrodt, W. Schlabitz, E. Holland-Moritz, M.M. Abd-Elmeguid, H. Micklitz, D. Johrendt, V. Keimes, A. Mewis, Z. Phys. B 98 (1995) 75.
[4] F. Merlo, M. Pani, M.L. Fornasini, J. Alloys Compd. 232 (1996) 289.
[5] R. Pöttgen, R.-D. Hoffmann, R. Müllmann, B.D. Mosel, G. Kotzyba, Chem. Eur. J. 3 (1997) 1852.

[6] R. Müllmann, B.D. Mosel, H. Eckert, G. Kotzyba, R. Pöttgen, J. Solid State Chem. 137 (1998) 174.
[7] R. Pöttgen, D. Johrendt, Chem. Mater. 12 (2000) 875.
[8] C. Felser, S. Cramm, D. Johrendt, A. Mewis, O. Jepsen, G. Hohlneicher, W. Eberhardt, O.K. Andersen, Europhys. Lett. 40 (1997) 85.
[9] D. Johrendt, C. Felser, C. Huhnt, G. Michels, W. Schäfer, A. Mewis, J. Alloys Compd. 241 (1997) 21.
[10] R. Pöttgen, Z. Naturforsch. 50b (1995) 1181.
[11] J. Evers, G. Oehlinger, K. Polborn, B. Sendlinger, J. Alloys Compd. 182 (1992) L23.
[12] R. Pöttgen, R.K. Kremer, W. Schnelle, R. Müllmann, B.D. Mosel, J. Mater. Chem. 6 (1996) 635.
[13] R. Pöttgen, Th. Gulden, A. Simon, GIT Labor-Fachzeitschrift 43 (1999) 133.
[14] R. Pöttgen, A. Lang, R.-D. Hoffmann, B. Künnen, G. Kotzyba, R. Müllmann, B.D. Mosel, C. Rosenhahn, Z. Kristallogr. 214 (1999) 143.
[15] K. Yvon, W. Jeitschko, E. Parthé, J. Appl. Crystallogr. 10 (1977) 73.
[16] (a) O.K. Andersen, Phys. Rev. B 12 (1975) 3060;
(b) O.K. Andersen, Europhys. News 12 (1981) 4;
(c) O.K. Andersen, in: P. Phariseau, W.M. Temmerman (Eds.), The Electronic Structure Of Complex Systems, Plenum Publishing Corporation, New York, 1984;
(d) O.K. Andersen, O. Jepsen, Phys. Rev. Lett. 53 (1984) 2571;
(e) O.K. Andersen, O. Jepsen, M. Sob, in: M. Yussouf (Ed.), Electronic Band Structure and Its Application, Springer, Berlin, 1986;
(f) H.L. Skriver, The LMTO Method, Springer, Berlin, 1984.
[17] U. von Barth, L. Hedin, J. Phys. C. 5 (1972) 1629.
[18] O. Jepsen, O.K. Andersen, Z. Phys. B 97 (1995) 35.
[19] P.E. Blöchl, O. Jepsen, O.K. Andersen, Phys. Rev. B 49 (1994) 16223.
[20] R. Dronskowski, P.E. Blöchl, J. Phys. Chem. 97 (1993) 8617.
[21] O. Jepsen, O.K. Andersen, personal communication.
[22] (a) G. Kresse, J. Hafner, Phys. Rev. B 47 (1993) 558;
(b) G. Kresse, J. Hafner, Phys. Rev. B 49 (1994) 14251;
(c) G. Kresse, J. Furthmüller, Comput. Mater. Sci. 6 (1996) 15;
(d) G. Kresse, J. Furthmüller, Phys. Rev. B 54 (1996) 11169.
[23] P.E. Blöchl, Phys. Rev. B 50 (1994) 17953.
[24] J.P. Perdew, K. Burke, Y. Wang, Phys. Rev. B 54 (1996) 16533.
[25] B.D. Oniskovets, V.K. Bels'kii, V.K. Pecharskii, O.I. Bodak, Sov. Phys. Crystallogr. 32 (1987) 522.
[26] K. Klepp, E. Parthé, Acta Crystallogr 38B (1982) 1541.
[27] L. Pauling, The Nature of the Chemical Bond and the Structure of Molecules and Crystals, Cornell University Press, Cornell, 1960.
[28] J. Emsley, The Elements, Oxford University Press, Oxford, 1999.
[29] J. Donohue, The Structures of the Elements, Wiley, New York, 1974.
[30] T.A. Albright, J.K. Burdett, M.-H. Whangbo, Orbital Interactions in Chemistry, Wiley, New York, 1985.
[31] (a) P.K. Mehrotra, R. Hoffmann, Inorg. Chem. 17 (1978) 2187;
(b) K.M. Merz, R. Hoffmann, Inorg. Chem. 27 (1988) 2120;
(c) A. Vega, V. Calvo, E. Spodine, A. Zarate, V. Fuenzalida, J.-Y. Saillard, Inorg. Chem. 41 (2003) 3389.
[32] (a) A.D. Becke, N.E. Edgecombe, J. Chem. Phys. 92 (1990) 5397;
(b) A. Savin, R. Nesper, S. Wengert, T.F. Fässler, Angew. Chem. Int. Ed. 36 (1997) 1808 and references therein.
[33] V.I. Anisimovy, F. Aryasetiawanz, A.I. Lichtenstein, J. Phys.: Condens. Matter 9 (1997) 767.
[34] A. Szytuła, J. Leciejewicz, Handbook of Crystal Structures and Magnetic Properties of Rare Earth Intermetallics, CRC Press, Boca Raton, FL, 1994.
[35] R. Pöttgen, J. Mater. Chem. 6 (1996) 63.
[36] T. Ito, S. Nishigori, I. Hiromitsu, M. Kurisu, J. Magn. Magn. Mater. 177–181 (1998) 1079.
[37] U. Ernet, R. Müllmann, B.D. Mosel, H. Eckert, R. Pöttgen, G. Kotzyba, J. Mater. Chem. 7 (1997) 255.